Single-Event Upsets in Photoreceivers for Multi-Gb/s Data Transmission

Alberto Jimenez Pacheco, Jan Troska, Luis Amaral, *Member, IEEE*, Stefanos Dris, Daniel Ricci, Christophe Sigaud, François Vasey, *Member, IEEE*, and Paschalis Vichoudis

***Abstract*—A Single-Event Upset study has been carried out on p-i-n photodiodes from a range of manufacturers. A total of 22 devices of 11 types from six vendors were exposed to a beam of 63 MeV protons. The angle of incidence of the proton beam was varied between normal and grazing incidence for three data rates (1.5, 2.0 and 2.5 Gb/s).**

We report on the cross-sections measured as well as on the detailed statistics of the interactions that we measured using novel functionalities in a custom-designed Bit Error Rate Tester. We have observed upsets lasting for multiple bit periods and have measured, over a large range of input optical power, a small fraction of errors in which an upset causes a transmitted zero to be detected as a one at the receiver.

***Index Terms*—Optical fiber communication, optical receivers, photodiodes, radiation effects.**

I. Introduction

SINGLE Event effects have been widely documented to occur in the photodiodes typically used in modern high-speed serial communications [1]–[4]. Particles traversing the material of the photodiode may deposit energy by direct ionization or via elastic and inelastic collisions with the nuclei of the material. Energy deposited by these mechanisms can lead to the formation of electron-hole pairs that are collected by the attached transimpedance amplifier (TIA) in the same way as the signal current associated with the data transmission. The transmission of a digital zero may thus be corrupted by the reception of a one caused by the additional energy deposited in this manner.

At CERN, we are currently designing the next generation of optical data transmission link for reading-out and controlling particle physics detectors to be operated at CERN's upgraded Large Hadron Collider (Super LHC). Such links will likely operate at multi-gigabit per second data-rates. The innermost regions of the detectors will encounter a radiation environment dominated by high-energy pions with a most-probable energy around 300 MeV, at fluxes of $10^6 - 10^8$ particles/cm^2/s, depending upon position with respect to the beam.

The control information flowing into the detectors from shielded control rooms is critical for maintaining the synchronization of the data-taking system, both internally and with respect to the bunched beams circulating in the SLHC. It is therefore of utmost importance that this control information be transmitted error-free and, with the knowledge that Single Event Upsets (SEUs) will occur within a photodiode placed in such an environment, the use of Forward Error Correction (FEC) coding will be mandatory. Validation of any choice of FEC code depends upon a detailed knowledge of the statistics of the errors that are expected to be encountered and the test reported in this paper aims to gather that knowledge.

Previous work by Marshall *et al.* has shown indications that a single error event can corrupt multiple data bits when the Device Under Test (DUT) is irradiated with 18 MeV Helium ions [2], [3]. Detailed statistics were not published in the above-mentioned study, which led us to design a test that would be able to measure these statistics in order to be able to design a FEC code that is robust against the SEUs expected in SLHC detector systems.

In order to gather as much information as possible, we performed a small survey of the radiation-response of several different devices. Single-Mode (SM) InGaAs p-i-n photodiodes operating at 1310 nm and Multi-Mode (MM) GaAs p-i-n photodiodes operating at 850 nm were combined in this test with Receiver Optical Sub-Assemblies (ROSA) where the TIA is mounted in the same TO-can as the photodiode. Again, both 1310 nm SM InGaAs and 850 nm MM GaAs ROSAs were included.

II. SEU Test Method

A. Irradiation Test Setup

The test aims to provide confirmation of the necessity of using FEC in the SLHC environment as well as a qualitative indication of the relative immunity of different device types to SEU. Since we do not aim to predict the exact Bit Error Rate (BER) that will be observed in the final system, the choice of using a relatively convenient proton facility was made. It is clear that the performance in the final (primarily pion-dominated) radiation field may have to be measured in a second step using a more representative beam in terms of both particle species and energy. The irradiation was carried out at the PIF-NEB proton irradiation facility at the Paul Scherrer Institut (PSI), Villigen, Switzerland [5] using a 63 MeV proton beam. The proton beam is pulsed with a repetition frequency of 51 MHz, each proton bunch lasting less than a nanosecond. The proton flux was 90% uniform over a radius of approx. 5 cm, which allowed the arrangement of eight photodiodes within the beam spot to be tested simultaneously. The tests were carried out at a flux of approx. 8×10^8 p/cm^2/s, which is equivalent to 16 protons per

Manuscript received September 09, 2008; revised December 09, 2008. Current version published August 12, 2009.

The authors are with CERN, CH-1211 Geneva 23, Switzerland.

Digital Object Identifier 10.1109/TNS.2009.2021836

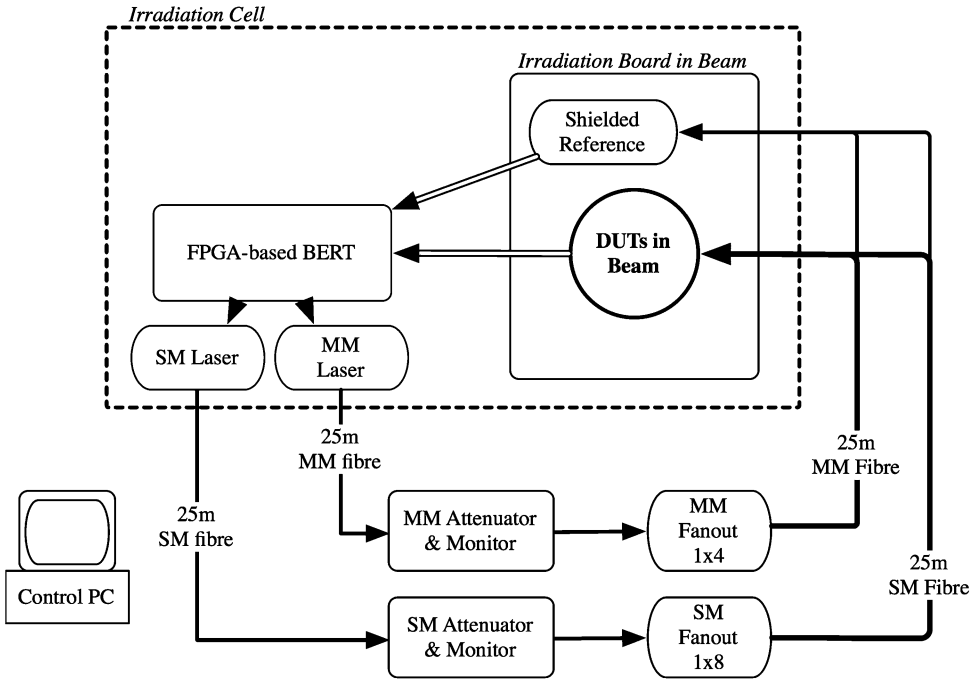

Fig. 1. Setup for the proton irradiation test.

bunch and square centimetre. Every second the flux was measured by ionization chambers and its value stored in a file by the control software of the irradiation facility for later analysis.

Data were generated as described in Section II.C inside an FPGA-based Bit Error Rate Tester (BERT) that was sited below the beam axis inside the irradiation bunker, but shielded with a combination of Aluminium and Polyethylene. The serial data was then fed to a laser driver and laser diode for conversion to an optical signal (see Fig. 1). This signal passed through 25 m of optical fiber to the control room, where an optical attenuator and power meter were used to control and measure the amplitude of the light returning, via an optical splitter and another 25 m of optical fiber cable, to the DUTs in the irradiation bunker.

The signals from the photodiodes require amplification in order to be sent over coaxial cables to the shielded BERT. Combined TIA/Limiting Amplifiers from Maxim Semiconductor (MAX3866) were mounted in very close proximity to the photodiodes on the test board. The electrical signals from the ROSAs were further amplified using a Limiting Amplifier (LA), also from Maxim Semiconductor (MAX3748B).

B. Devices Tested

Devices were selected based upon current availability from six vendors. Table I shows the devices tested and some relevant parameters. One device type (D1) was included to provide a comparison with previous work carried out at CERN [4] at lower data-rates.

The devices were arranged across three test boards that were exposed in succession to the proton beam. A photograph of a test board set up in the beam line is shown in Fig. 2. The active devices were shielded from the proton beam by 6.5 mm of brass. In addition, each set of eight DUTs exposed to the beam was accompanied by two reference photodiodes and TIA/LAs

TABLE I
DEVICES TESTED. SINGLEMODE (SM) DEVICES WERE TESTED AT 1310 NM AND MULTIMODE (MM) DEVICES AT 850 NM.

Family	Device Type (# tested)	Active diameter	Responsivity measured
PIN SM	A1 (2)	30μm	0.7 A/W
PIN SM	A2 (2)	60μm	0.8 A/W
PIN SM	A3 (1)	60μm	0.75 A/W
PIN SM	A4 (2)	80μm	0.8 A/W
PIN SM	B1 (2)	60μm	0.8 A/W
PIN SM	C1 (2)	80μm	0.75 A/W
PIN SM	D1 (3)	80μm	0.8 A/W
PIN MM	E1 (2)	100μm	0.6 A/W
PIN MM	F1 (2)	90μm	0.6 A/W
ROSA SM	F2 (2)	65μm	3.0 $mV_{pp}/\mu W$
ROSA MM	F3 (2)	90μm	2.2 $mV_{pp}/\mu W$

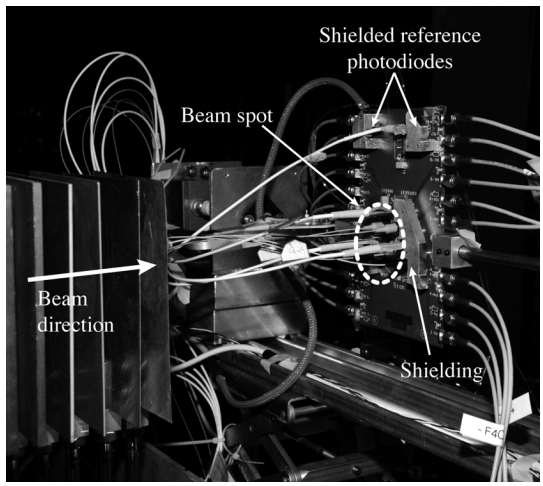

Fig. 2. Photograph of one of the irradiation boards mounted on the rotating axle. There are 8 DUTs on the beam spot.

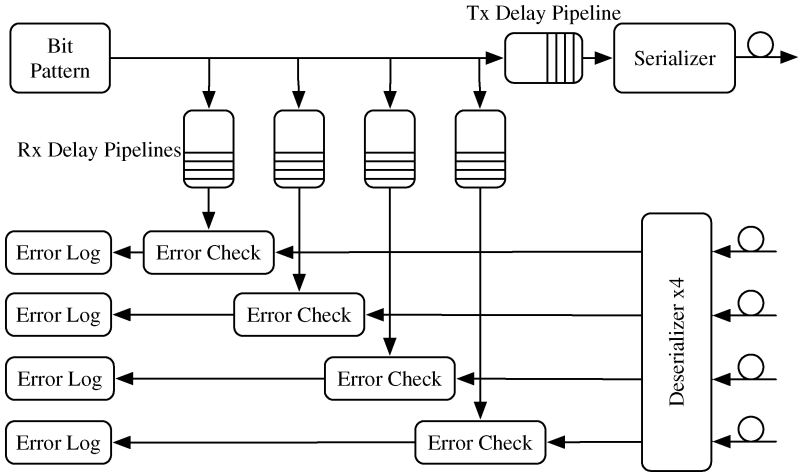

Fig. 3. Simplified diagram of the BERT implemented in firmware.

that were completely shielded. These references, one SM (D1) and one MM (E1), were provided to measure any possible noise induced by external sources within the irradiation bunker. The DUTs were mounted on a rotating axle that allowed the angle of incidence of the proton beam on the optoelectronic receivers to be varied between normal (0°) and grazing incidence (90°) by remote control from outside the irradiation bunker. Measurements were taken at 0°, 10°, 80° and 90°.

C. FPGA-Based Bit Error Rate Tester

A custom BERT was implemented based upon the Transceiver Signal Integrity Development board available from Altera for the Stratix II GX family of FPGAs, which include embedded high-speed transceivers capable of transmitting and receiving Non-Return to Zero (NRZ) data at rates up to 6.375 Gb/s [6].

A memory of 8 K 20 bit words contained the pattern cyclically sent using NRZ signalling by the transmitter. In our case this memory was filled with random data, 8B/10B encoded offline for line-balancing and with commas inserted every 64 words to aid synchronization in the receiver. The received data were compared "as-is", i.e., not decoded, to measure the raw BER due to SEU errors only and not errors due to decoding problems.

To enable measurement of error statistics an error log memory that could hold up to 8 K 20 bit words was implemented. For every received word, the XOR of the transmitted and received data was evaluated and if one or more bit errors were detected, this error pattern was stored in the memory. An absolute timestamp corresponding to the error word is also stored. In addition, basic Bit Error, Word Error and transmitted Word counters were implemented. Bit Error Rate is then calculated as the ratio of detected Bit Errors over the total number of transmitted bits.

Firmware was developed that would allow operation at the three data rates used in the test (1.5, 2.0 and 2.5 Gb/s) by simply supplying a different frequency base clock to the FPGA. The firmware schematic shown in Fig. 3 shows that each BERT contained one transmitter and four receiver channels. In order to reach the required channel count of ten devices per test board, three BERTs were used simultaneously: one pair in master/slave configuration with a single transmitter and eight receivers; and the third in the standard one transmitter to four receiver configuration.

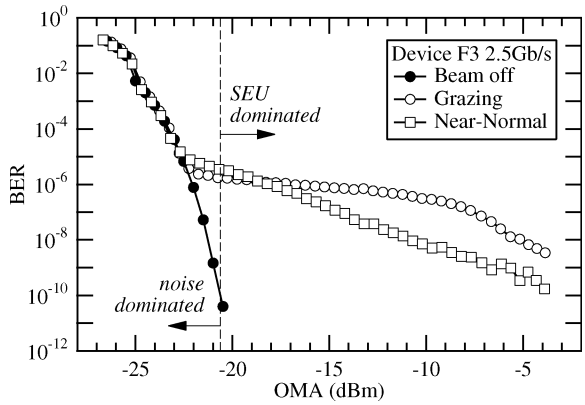

Fig. 4. Illustration of the effect of the proton beam for two different incident angles on the observed Bit Error Rate with respect to beam off data.

III. Results: Overall Trends

For every combination of the selected data rates and angles, attenuation scans monitoring the BER were systematically performed both with the beam on and off, to be able to distinguish in every case errors caused by protons from those due to electrical and environmental noise.

As an example, in Fig. 4 we show the effect that turning on the beam has on the BER performance of a ROSA (F3). In this figure and throughout the paper, the Optical Modulation Amplitude (OMA) is the signal amplitude at the input of the optoelectronic receivers that is obtained by correcting the power measured by the online monitor (Fig. 2) for the transmission losses in the measurement system. When the beam is on, the range of OMA can be divided in two regions, one where performance is dominated by noise and one where it is dominated by radiation induced errors. The excellent matching in the noise dominated region between the plots with beam on and off shows the good reproducibility of the results.

Fig. 4 shows the additional effect on the BER curve of changing the incident beam angle from grazing (90°) to

near-normal (10°). The excess BER observed at grazing incidence has been shown by the simulations performed in [4] to be due to the ionization component of the energy loss of the particles in the photodiode material. At high OMA, in fact almost beyond the reach of the transmitter power available in this test, the two curves would be expected to meet as sufficiently high energy loss to compare to high optical signal amplitude can only be caused by nuclear interactions where the energy loss is essentially independent of angle.

Plots similar to that of Fig. 4, comparing the BER with beam off and on, were analysed for the reference photodiodes at all incidence angles. These have shown that the shielding was not working perfectly at all angles; specifically, some upsets could be observed in the reference photodiodes near grazing incidence.

In the following, most results will be presented in terms of the Bit Error Cross Section, defined as the quotient between the number of bit errors occurring during the testing time and the accumulated fluence. This cross section is only defined and presented in the SEU dominated region that is taken to be the region for which the OMA exceeds that required to achieve a BER of 10^{-10} with the beam off. For all the data presented in what follows, the measurement uncertainty can be taken to be equivalent to the marker size used in the plots. Due to the large number of different devices tested we show data that are representative of the behaviour of all tested devices unless stated explicitly in the accompanying text.

The DUTs were exposed to a total proton fluence between 1×10^{13} p/cm^2 and 2.4×10^{13} p/cm^2. From our observation that the beam-off noise limit does not shift significantly during the test we conclude that the total fluence received during the test had little appreciable influence on the DC-characteristics (responsivity, leakage current) of the DUTs.

A. Device Families

In Fig. 5 we compare the Bit Error Cross Section of every model used in our test under a common set of conditions, 2.5 Gb/s and grazing incidence (90°). For a given value of OMA the difference in cross section among devices spans more than two orders of magnitude, but the plots for all models exhibit the same general shape. The variety of active diameters, packaging materials and manufacturing processes among devices from different manufacturers makes general trends difficult to observe.

Nevertheless, photodiode A1, which happens to have the smallest active diameter of all the devices tested (30 μm), stands out as remarkably better than the rest. Since the path of the protons through the active volume is minimised, so is the BER, especially the contribution due to direct ionization.

The ROSAs do not rank among the devices with worse performance (especially for the single mode case), even though in these devices we are certain to be observing the combined effects of SEUs in the photodiode and in the unshielded TIA (the LA is shielded).

B. Angular Dependence

We confirm the observation made in previous tests by other authors [1], [2] and our own team [4]: that the maximum of

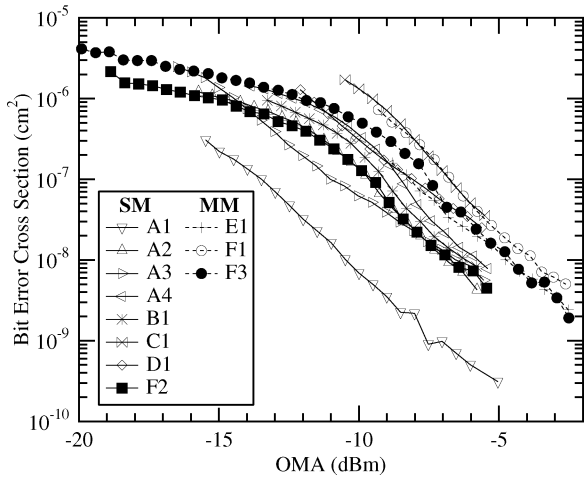

Fig. 5. Overview of results for all devices at 2.5 Gb/s and 90°.

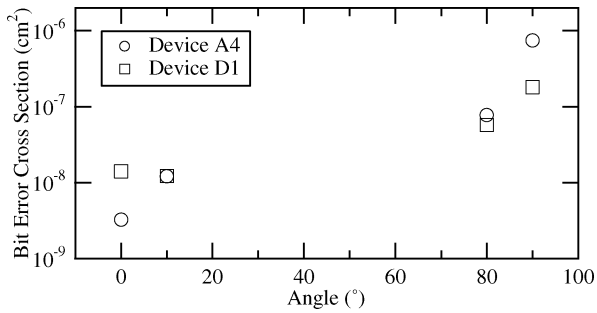

Fig. 6. Bit error cross section as a function of received optical power for two devices tested at 2.5 Gb/s and different angles.

the cross section as a function of the incidence angle occurs near 90° (grazing incidence) and it is minimum for 0° (normal incidence), as shown in the example of Fig. 6. This is expected, as 90° corresponds to the longest ionizing path of the protons through the active volume of the photodiode.

The distance that the protons travel through the device decreases very quickly as we move away from grazing incidence, and since the charge generated by direct ionization is reduced proportionally, we were expecting a very selective peak of the cross section around 90°, as shown for instance in [1] or [4]. However that is not exactly what we observe in Fig. 6, where the points corresponding to 0° and 10° should be closer to one another, and closer to that of 80°, to agree with this expectation. This deviation from the expected behaviour could be explained by partial shadowing of the DUTs by the optical fibers and connectors attached to them, which could degrade the energy of the beam for angles at normal incidence (see Fig. 2).

C. Data Rate Dependence

It is important to understand the dependence of the BER on the rate of data transmission since, for example, simply lowering the data-rate to achieve lower SEU-induced BER could provide an easily-implementable method to recover system margin if this behaviour were observed.

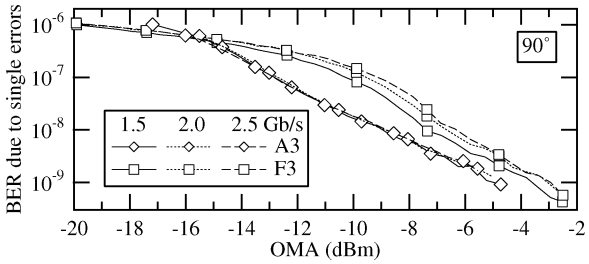

Fig. 7. Bit error rate due to isolated single bit flips as a function of received optical power for two devices at 2.5, 2.0 and 1.5 Gb/s; grazing incidence.

With this in mind, using the following relationship [3] between BER, Bit Error Cross Section (σ), data rate (R) and average flux (ϕ):

$$\mathrm{BER} = \frac{\sigma \times \phi}{\mathrm{R}} \tag{1}$$

we would conclude that if the cross-section were to depend linearly on data-rate, then the BER would be independent of it and no gain of the type outlined in the example above would be possible. In Fig. 7 we plot the BER due to isolated single bit errors for two devices at the same incident proton angle for the three data rates tested. We have chosen the BER due only to isolated single bit errors in an attempt to show what might be possible to achieve in the absence of effects due to the receiving amplifier chain. From this plot we would conclude that the photodiode behaves differently from the ROSA in that they appear to show that the BER is independent (within the measurement uncertainty) of data-rate for the range of rates used in this test.

However, as shown in Fig. 8 where we take a cut through the cross-section equivalent of Fig. 7 at a particular OMA and normalize the result to the value at 1.5 Gb/s to ease the comparison, we can see that none of the devices in fact show a linear behaviour. Devices A3, C1 and F3 exhibit a slight 'super-linear' dependence of cross-section on data-rate whereas device B1 appears to show a non-linear behaviour that 'saturates' at higher data-rates, the former being similar to the behaviour shown in [7]. Detailed conclusions are however difficult given the limited range of data-rates used in this test and we cannot generalise which device types show which type of behaviour. This tells us that testing at the chosen data-rate will be mandatory in a future test to establish the final SEU-induced BER.

IV. Results: Error Log Analysis

The error logging mechanism implemented in the custom FPGA BER Tester allows us to obtain a very detailed analysis of the error statistics: Error Free Interval (EFI) histograms, burst length histograms, as well as correlation of errors with the transmitted pattern.

In order to characterise an error burst, not only is its length important, but also the value of the Error Free Threshold (EFT) used in the analysis [8], [9], defined as the maximum number of successive correct bits allowed inside a burst. The value of the EFT must be carefully selected, examining simultaneously its effect both on the EFI histogram and on the burst histogram. On one hand, the EFT must be high enough so that all bit flips

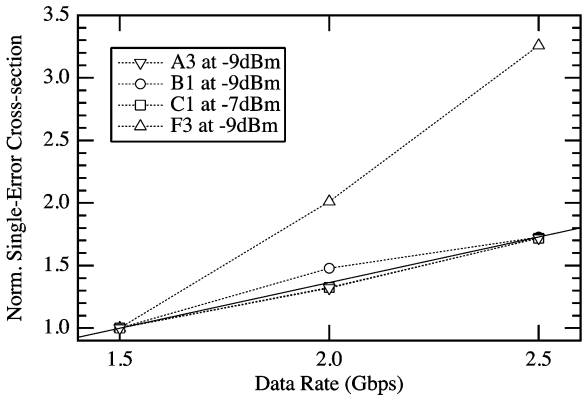

Fig. 8. Cross-section equivalent of Fig. 7 for isolated single bit errors normalized to the value at 1.5 Gb/s as a function of data-rate at constant OMA. A straight line to guide the reader's eye has been included.

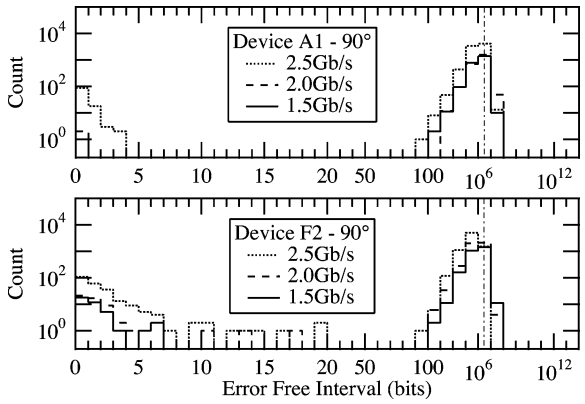

Fig. 9. Example EFI histograms with $\mathrm{EFT} = 0$ that are representative for Photodiodes (top) and ROSAs (bottom). The dot-dash line represents 1/BER for reference.

originated by the same physical cause are grouped as a single burst, independently of *lucky* correct bits inside the burst; on the other hand, it must be low enough so that errors induced by different events are not grouped together in a single long burst. For instance, in order not to group errors caused by protons from different accelerator bunches, the EFT should be less than 29 at 1.5 Gb/s, or less than 49 at 2.5 Gb/s.

At a given OMA value, the centre of gravity of the EFI histogram should be close to the inverse of the BER measured at that point as illustrated in Fig. 9. If important contributions to the EFI histogram appear for values much lower than 1/BER, this tends to indicate that the EFT is too low, especially if there is a discontinuity between these two important masses in the histogram. This is again illustrated in Fig. 9, which shows a reasonably significant population of events where the EFI is rather short – indicating that these events are likely to be part of longer error bursts. We have obtained satisfactory results by selecting an EFT of 10 bits for the photodiodes and 40 bit for the ROSAs, implying that any two bit-errors separated by 10 (40) or fewer correct bits are considered part of the same burst.

A. Error Classification

We have used the results from the error log analysis to classify the errors according to the following criteria:

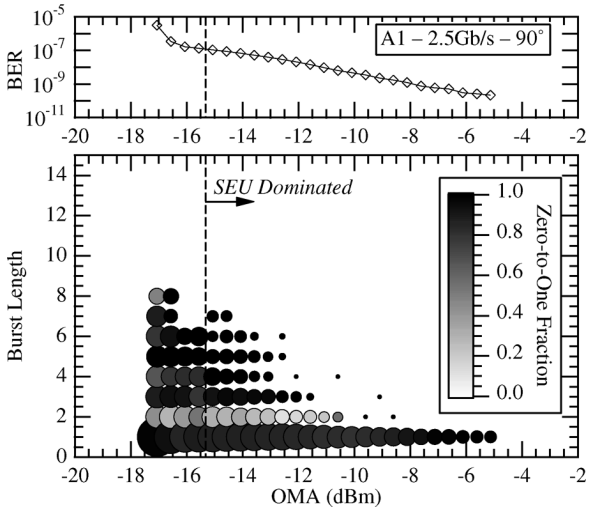

Fig. 10. Two-dimensional burst histogram for Device A1 tested at 2.5 Gb/s and grazing incidence. $\mathrm{EFT} = 10$ bits.

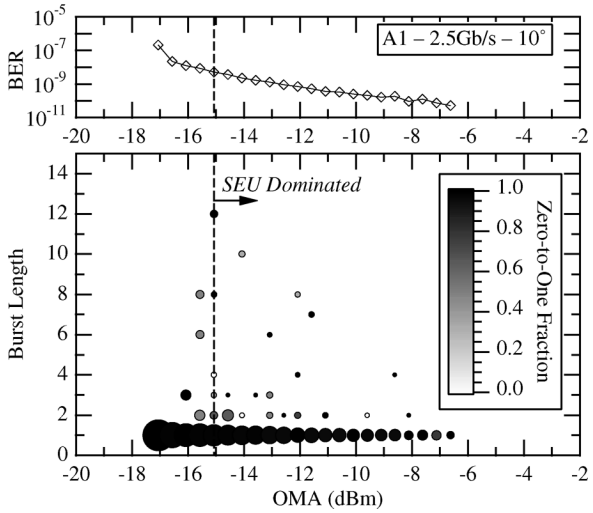

Fig. 11. Two-dimensional burst histogram for Device A1 tested at 2.5 Gb/s and near-normal (10°) incidence. $\mathrm{EFT} = 10$ bits.

- **Error length**. We distinguish between single (isolated) errors and burst errors.
- **Fraction of 0-to-1 errors**. We can correlate the logged error patterns with the transmitted sequence to find out what fraction of the bit errors are due to sent zeros being mistaken at the receiver as ones and vice-versa.
- **Burst occupancy** (sometimes also termed burst density): is computed as the number of bits that were actually flipped in a burst divided by the length of that burst.

For a given set of test conditions (data rate, angle), a convenient way to simultaneously visualize the burst histograms of a device for the complete range of attenuation values tested is what we call a two-dimensional colour-coded burst histogram, for which we show several examples in Fig. 10 (Photodiode at grazing incidence), Fig. 11 (Photodiode at near-normal incidence) and Fig. 12 (ROSA at grazing incidence). In the lower plot, burst lengths are represented in the axis of ordinates and power levels in the axis of abscissa. A circle is drawn at point (x, y) if one or more bursts of length y bits are present in the 1D-burst histogram for a received power level of x (dBm). The size of the circle is logarithmically proportional to the BER contribution due to all bursts of length y at this power level. The colour of the circle gives information about the average 0-to-1 fraction or burst occupancy, following the colour scale shown to the right of the figure. The upper plot of each figure shares the axis of abscissa with the lower one, and shows the dependence of the total BER on OMA.

Data at grazing incidence contain SEUs generated mostly by directed ionization, whereas the data at near-normal contain (in relative terms) more events that are due to nuclear interactions. This distinction becomes important when we consider the relevance of the data presented here to radiation environments that are not proton-dominated. Near-normal has been chosen to avoid the experimental problem that the DUTs were shielded by their input fibers at normal incidence, which led to the artificial reduction in SEU rate shown in Fig. 6.

Making a global classification of the errors required the careful examination of this kind of 2-D histogram for all

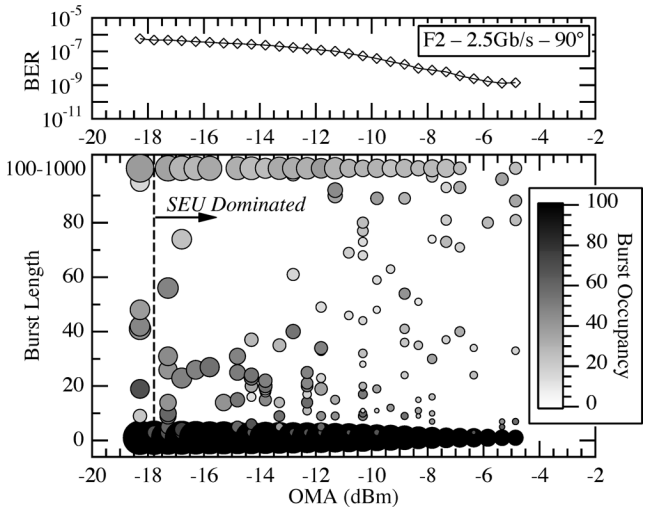

Fig. 12. Two-dimensional burst histogram for Device F2 tested at 2.5 Gb/s and grazing incidence. $\mathrm{EFT} = 40$ bits.

devices and test conditions, but the examples presented here are representative of the general behaviour of photodiodes and ROSAs, respectively. Therefore, we will refer to the examples in Figs. 10–12 to illustrate many of the general conclusions that we present next.

We can classify the errors induced by SEU in three groups:

1. **Single errors**: this is by far the dominant type of error as shown in Figs. 13 and 14. Independently of the device, data rate, angle or power level, the bin of length 1 dominates all burst length histograms. Almost all single errors are due to 0-to-1 bit flips. Although not shown here, we measured that at the OMA limit where SEUs begin to dominate the BER, the probability of a noise-induced 1-to-0 error is below 10^{-12} and falling by two decades per dBm. Within the SEU dominated region, 1-to-0 bit flips nevertheless occur at the level of a few per cent (photodiodes) or a few per mille (ROSAs). This can be seen more clearly in Figs. 13 and 14, where the contributions to the total BER of different

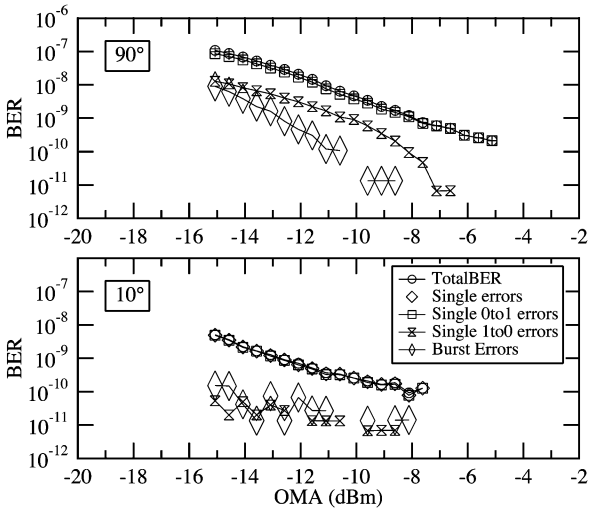

Fig. 13. Contributions to the BER from different error types as classified in the main text for Device A1 at 2.5 Gb/s for grazing incidence (90°) (upper plot) and near-normal incidence (10°) (lower plot).

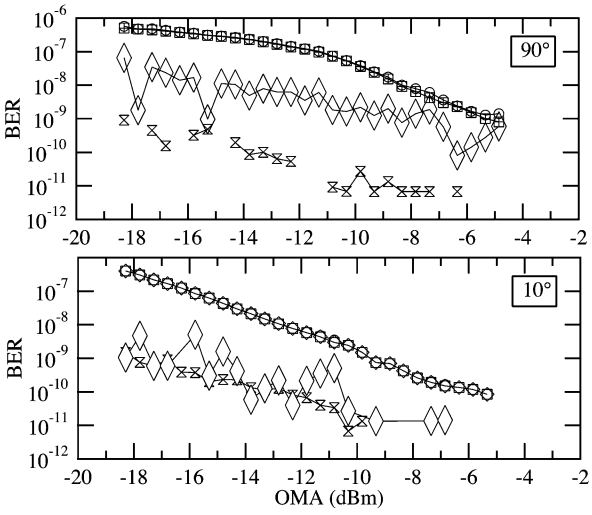

Fig. 14. Contributions to the BER from different error types as classified in the main text for Device F2 at 2.5 Gb/s for grazing incidence (90°) (upper plot) and near-normal incidence (10°) (lower plot). Legend as for Fig. 13.

types of errors have been represented for the same devices and test conditions as in Figs. 10–12. The incident proton angle appears to have a large influence on the rate of 1-to-0 errors in photodiodes, as shown in Fig. 13 where the relative rate of these errors can be seen to be an order of magnitude lower at near-normal than at grazing incidence. However, there appears to be less influence of the incident angle on the 1-to-0 rate in ROSAs than photodiodes.

It is generally stated in the literature that SEUs in photodiodes can only be produced as 0-to-1 transitions. In this test we are necessarily observing bit errors that result from the combined response to a particle strike of the photodiode and the TIA/LA. As we do not have access to a detailed device model of the TIA/LA from the manufacturer, we can but hypothesise that the observed 1-to-0 transitions are due to a non-linear response of the amplifier to the particle-induced charge deposition in the photodiodes. The different behaviours between photodiodes and ROSAs might be explained by the use of different amplifiers in the two types of devices (the ROSAs include a TIA 7770 from Vitesse Semiconductors integrated with the photodiode in the TO-can).

2. **Short bursts (2–20 bits)**: For this type of error the conclusions differ slightly between ROSAs and the rest of devices:
   - For photodiodes there is a strong correlation between the optical power at the receiver input and the occurrence of this type of burst: the lower the power, the higher the number of bursts, and also the more important their contribution to the total BER. With respect to the 0-to-1 fraction, similarly to what happened for single errors, it is very close to 1. Many of the photodiodes show an anomaly by which all short bursts have a high 0-to-1 fraction except bursts of length 2. This is for example the case for the SM device in Fig. 10, for which most double errors are in fact pairs of 1's mistaken in the receiver as pairs of 0's. This behaviour is still under investigation.
   - For ROSAs, there is also a high correlation of the short bursts with the power level, but it is more irregular and, contrary to photodiodes, a few short bursts are still present for very high values of the received power. With respect to the 0-to-1 fraction, in the ROSAs it is higher than for photodiodes, almost exactly equal to 1. There is no anomaly affecting the 0-to-1 fraction for double errors.

   It is especially interesting that for both types of device the occupancy of these bursts is close to 100%. This is the first direct measurement of multiple-bit bursts in photoreceivers reported in the literature.

   We have also observed, both for photodiodes and ROSAs, that the contribution of short bursts to the total BER is strongly correlated with angle: short bursts occur more often at 90° than at 80°, and more often at 80° than at 10°; they almost disappear when the angle approaches 0°.

   With an average flux of 8×10^8 p/cm^2/s, a pulse repetition frequency of 51 MHz, and the small active diameters of the devices tested, the probability that different protons from the same bunch hit a given device in neighbouring bit periods is in the range 5×10^{-4} to 5×10^{-3}. Thus, a possible overestimation of the short bursts is excluded.
3. **Long bursts (length $>$ 20 bits)**, which are almost exclusively present in the ROSAs. The main characteristic of this type of error is that the burst occupancy is low, around 30-40%. The 0-to-1 fraction is very close to 1, as was also the case for single errors and short bursts in the ROSAs.

   Long bursts are to some degree correlated with the received power level, as shown by the plot of their contribution to the total BER in Fig. 14. However, a quick look at Fig. 12 also reveals that long bursts can basically occur for any value of OMA.

   We have also observed some dependence on angle: many fewer long bursts occur around normal incidence than at grazing as shown in Fig. 14.

In Fig. 12 we see that the distribution of burst lengths is more or less continuous, without a gap between short and long bursts. Short bursts actually occur in ROSAs more frequently than long ones, but even so the contribution of the long ones to the total BER is much more important. This is because, despite their low occupancy, long bursts can last up to a few hundred bits (In Fig. 12 we limited the range shown for clarity). In contrast, bursts longer than 10 bits are very rare in photodiodes (Figs. 10 and 11).

As for the reference devices, we almost exclusively observed single errors, and a few short bursts at very low power levels, induced by noise. The very few short bursts occurring at higher power levels can be explained by the fact that the shielding was not working perfectly for angles near grazing incidence, as mentioned in Section III.

B. Hypothesis for the Origin of Bursts

We hypothesise that the long bursts occurring in the ROSAs are due to upsets taking place in the TIA, rather than in the photodiode. The fact that long bursts are almost exclusively present in the ROSAs, where the TIA cannot be shielded, supports this hypothesis; on the other hand, the very few long bursts that appear on photodiodes could still share the same origin because the shielding was not completely effective.

Another fact that backs up this theory is that the median length of long bursts, when expressed in absolute time units (ns, rather than bit periods), turns out to be fairly independent of the data rate. It takes values around 50-60 ns. These events are very long compared to the speed of the TIA, so probably the errors are not due to hits in the signal path but to hits in other nodes of the circuit with much longer time constants.

One fact that would contradict this hypothesis is the observed angular dependence, because it would point to direct ionization as the fundamental mechanism responsible for the bursts, and it is unlikely that 60 MeV protons could affect any internal node by direct ionization. Nuclear interaction with the materials in the integrated circuit seems a more plausible physical mechanism, but recoils would only show a marginal angular dependence.

To investigate in more detail if there indeed is an angular dependence or not, we have calculated the cross section for long bursts (σ^*), defined as the number of long bursts divided by the fluence (i.e., each long burst counts as one error event independent of its length). In Fig. 15 we represent σ^* for a MM ROSA as a function of OMA for different angles, and we verify that the long error cross section is indeed fairly independent of angle, except for 0°. However this lower cross section could be explained by the partial shadowing of the devices by the fibers and connectors at angles near normal incidence. Similar results are obtained for the SM ROSAs and at other data rates, which reinforces our hypothesis that SEUs in the TIA could be at the origin of long bursts.

In contrast, we favor the hypothesis that short bursts are indeed related to upsets in the photodiodes, since we observed a very marked dependence on the received power level and on the incidence angle, the occupancy of these bursts is quite high and the majority of the bit flips correspond to 0's turning into 1's. We have not found a fully convincing explanation for anomaly of 2-bit bursts being predominantly of the 1-to-0 type that has been observed in several models of photodiode and is visible in Fig. 10. This anomaly may be due to an overly long recovery time of the TIA/LA in response to a very large signal at its input, but this cannot be verified in the absence of a detailed simulation model of the amplifier that is unfortunately not available to us.

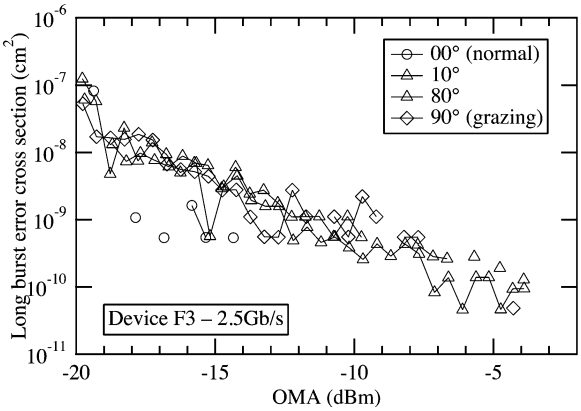

Fig. 15. Long burst error cross section of a MM ROSA for different angles. 2.5 Gb/s. Each burst longer than 30 bits counts as a single error for the definition of cross section.

V. Conclusions

Results of an ambitious SEU test with protons of a large selection of P-I-N photodiodes and ROSAs operating at high data rates have been presented. Tests at various incidence angles have confirmed that the highest error cross sections are obtained for angles near grazing incidence. A number of device types have shown an independence of the SEU-induced BER on data-rate, whereas for others the SEU cross-section was observed to saturate at the highest data-rates tested.

The use of a custom BER tester allowed us to obtain detailed statistics of the error events. For instance, isolated errors in which a transmitted 1 is detected as a 0 at the receiver have been observed at power levels where they are very unlikely to have been induced by electrical noise.

We have also shown that multiple bit errors can occur in optoelectronic receivers. Short error bursts spanning up to a dozen bits were observed in the photodiodes and longer bursts, up to a few hundred bits in length, have been measured in the ROSAs. To the best of our knowledge, this kind of behaviour, where an SEU can upset several successive bits, has not been previously reported in SEU tests performed with photoreceivers at other data rates. Short bursts could be originated by upsets in the photodiodes and the response of the attached amplifier to the sudden appearance of a signal significantly larger than the average. Long bursts in the ROSAs are most likely related to proton hits in the unshielded TIA. It seems probable, since we observed these effects for all DUTs, that other combinations of photodiode and TIA not tested here will show the occurrence of similar burst errors.

Burst errors will have to be mitigated using FEC coding in future optical links to be used inside Super LHC detector systems if Bit Error Rates below 10^{-12} are to be guaranteed for all incident angles in the expected radiation field. The detailed statistics collected during this test will prove essential in the design

and validation of an appropriate FEC scheme, which is beyond the scope of this paper.

As this test was carried out using a proton beam to simulate a final environment likely to be dominated by pions, the final SEU rates likely to be observed at SLHC will have to be measured in a future test using a representative particle beam and the final data-rate chosen for the application. Moreover, the observed effects, in particular the unexpected 1-to-0 transitions and burst errors, are very likely due to the combined response of the photodiode and its amplifier to what may be a relatively large signal by comparison to the data signal. For this reason, additional testing with beam will be required to measure the response of a range of photodiodes combined with the radiation-tolerant TIA/LA currently being designed at CERN. Indeed the response of the amplifier may be designed in order to provide some direct mitigation of short burst errors by choice of architecture. In addition, the in-house design may be able to be tailored to provide immunity to long bursts now that the designers have been made aware of the issue.

ACKNOWLEDGMENT

The authors would like to thank Dr. W. Hajdas for his help during irradiation at PSI. We would also like to acknowledge the fruitful discussions held with Dr. F. Faccio, Dr. P. Moreira, Dr. J. Christiansen, Dr. P. Farthouat, Dr. A. Marchioro and Mr. C. Soos at CERN.

REFERENCES

[1] P. W. Marshall, P. T. Wiley, R. N. Prusia, G. D. Rash, H. Kim, and K. A. LaBel, "Proton-induced BiTerror studies in a 10 Gb/s fiber optic link," *IEEE Trans. Nucl. Sci.*, vol. 51, no. 5, pp. 2736–2739, Oct. 2004.

[2] P. W. Marshall, C. J. Dale, and K. A. LaBel, "Space radiation effects in high performance fiber optic data links for satellite data management," *IEEE Trans. Nucl. Sci.*, vol. 43, no. 3, pp. 645–653, Jun. 1996.

[3] P. W. Marshall, C. J. Dale, M. A. Carts, and K. A. LaBel, "Particle-induced bit errors in high performance fiber optic data links for satellite data management," *IEEE Trans. Nucl. Sci.*, vol. 41, no. 6, pp. 1958–1965, Dec. 1994.

[4] F. Faccio, G. Berger, K. Gill, M. Huhtinen, A. Marchioro, P. Moreira, and F. Vasey, "Single-event upset tests of an 80-Mb/s optical receiver," *IEEE Trans. Nucl. Sci.*, vol. 48, no. 5, pp. 1700–1707, Oct. 2001.

[5] W. Hajdas, A. Zehnder, L. Adams, and B. Nickson, "The proton irradiation facility at the Paul Scherrer institute," *Nucl. Instrum. Methods Phys. Res. B*, vol. 113, p. 54, 1996.

[6] Stratix II GX EP2SGX90 Transceiver Signal Integrity Development Board: Reference Manual Altera [Online]. Available: http://www.altera.com/literature/manual/rm_si_bd_2sgx90.pdf

[7] C. J. Marshall, P. W. Marshall, M. A. Carts, R. A. Reed, S. Baier, and K. A. Label, "Characterization of transient error cross sections in high speed commercial fiber optic data links," in *Proc. Radiation Effects Data Workshop*, 2001, pp. 142–145.

[8] E. A. Newcombe and S. Pasupathy, "Error rate monitoring for digital communications," *Proc. IEEE*, vol. 70, no. 8, pp. 805–828, Aug. 1982.

[9] D. J. Kennedy and M. B. Nakhla, "Burst error characterization of FEC coded digital channels," *Int. J. Satellite Commun.*, vol. 10, no. 5, pp. 243–250, 1992.